Quantitative analysis of flow dynamics of organic granular materials inside a versatile silo model during time-lapse X-ray tomography experiments

Laurent Babout, Krzysztof Grudzien, Selam Waktola, Konrad Miskiewicz, Jerome Adrien, Éric Maire

Quantitative analysis of flow dynamics of organic granular materials inside a versatile silo model during time-lapse X-ray tomography experiments

Laurent Babout [1,] *, Krzysztof Grudzień [1], Selam Waktola[1], Konrad Miśkiewicz[1], Jerome Adrien[2] and Eric Maire[2]

[1] Institute of Applied Computer Science, Lodz University of Technology, 18/22 Stefanowski st., 90-924 Lodz, Poland

[2] MATEIS INSA Lyon, Bat B Pascal, 7 Ave Jean Capelles, Villeurbanne, France

***** Correspondence: Laurent.babout@p.lodz.pl, Tel: +48 42 631 2750 (+305)

Abstract: gravitational flows, like silo discharge, vary in mode and are complex to identify since they depend on various parameters, ranging from silo structural properties to granular material properties. Moreover, the way cohesionless particles arrange themselves during the flow is still a matter of study and new experimental approaches are needed. Here, the paper introduces a new versatile silo model that was specially designed for in situ X-ray tomography studies of silo discharge for various flow conditions, namely concentric and eccentric. The presented work focuses on organic granular materials, i.e. sorghum and rice, which present relatively similar physico-mechanical properties but different elongation. The high-quality tomography images combined with adequate image processing strategy allow to unambiguously analyse individual grains dynamic behaviour during silo discharge for different hopper configurations. The paper focuses on the analysis of packing density, coordination number and grain rotation changes during funnel flow. The quantitative analysis essentially shows that hopper eccentricity and particle elongation influence flow dynamics of funnel flow. The proposed experimental methodology is proven to be solid enough to investigate in more detail dynamic phenomena during silo discharge. It can also serve as a strong baseline for numerical calibration and predictions.

Keywords: silo construction; asymmetric flows; funnel flow; 3D particle analysis; X-ray tomography.

1. Introduction

Silos and hoppers have been around in the industry for decades as efficient and reliable containers to store and transport granular materials. Depending on the applications, their size and shape change, ranging from small hoppers used for drugs dosage to large-scale silo to store organic granular materials. As far as the discharge process is concerned, it is still not completely known how to set strict design specifications for achieving a given discharge rate for a chosen type of granular material. Indeed, the choices of the outlet width and inclination of hopper are strongly linked with the particle geometry (size, shape), packing density and mechanical properties such as internal friction and cohesiveness of the granular material. These choices are also governed by the desired flow regime to be achieved, i.e. funnel flow, mass flow or mixed flow. While mass flow is usually chosen for material discharge optimization in agriculture, funnel flow is, for example, of interest in pebble-bed reactors where graphical pebbles are cycled through the core in a dense granular flow (Rycroft et al., 2006). While the majority of the studies have concerned classical symmetric silo design with one opening, recent works investigated less standard design, which propose more than one hopper opening (Cheng et al., 2010; Fullard et al., 2019), lateral orifice (Medina et al., 2014; Zhou et al., 2017), but also eccentric flow due to offset filling or hopper asymmetric design (Ayuga et al., 2001; Chou et al., 2002; Grudzień et al., 2018; Sadowski and Rotter, 2011; Sielamowicz et al., 2010). Numerical modelling is therefore often selected as the main decision-making solution for silo/hopper design in order to adapt to specific user's needs. While simulation has been envisioned in many situations to avoid experimental verifications, it still needs experimental comparisons to strengthen the physico-mechanical laws and approximations that made the foundation of the numerical calculations. For instance, the discrete element method (DEM), which is often used to model grain interaction, has shown good qualitative prediction potential, but, on the other hand, frequently failed to match quantitatively experimental measurements mainly due to model oversimplification

(González-Montellano et al., 2011). This could have different reasons: bad choice of granular materials property, initial packing distribution or particle shape that does not fully agree with experimental conditions. Moreover, intensive bibliographic research recently reviewed in Saleh et al. (2018) tends to show that the topics of predilection associated with granular flow in silos concern flow patterns, segregation, stress distribution, velocity profiles and discharge rate. However, no particular work is mentioned about the study of experimental or predicted evolutions of packing density or local concentration changes during discharge. Nonetheless, such information could be valuable to indirectly correlate with other parameters, for instance the dynamic stress field, by estimating local packing density and related coordination number. This is why numerical simulations need to be confirmed by experimental measurements, which not only focus on velocity fields and discharge rate, but also analyse upstream phenomena such as local concentration dynamics.

A majority of previous gravitational flow studies have considered fine granular material such as sand (Grudzien et al., 2012; Oldal et al., 2012; Slominski et al., 2007) and digital particle image velocimetry applied on optical images to characterize velocity shear zones (Sielamowicz et al., 2005; Slominski et al., 2007; Steingart and Evans, 2005; Szabó et al., 2018). Comparison between optical images and numerical simulation based on DEM was also widely used for organic materials (Balevičius et al., 2011; González-Montellano et al., 2011). However, all mentioned works only considered surface observations. This hinders the study of transversal movement of grains during silo emptying, especially when rough walls are used. The approach proposed in this work tries to circumvent the latter problem by studying silo discharge phenomena using X-ray tomography imaging. Indeed, this non-destructive method, which has been used in agriculture to characterize grains (Neethirajan et al., 2008), perform quality control on vegetables (Brecht et al., 1991; Donis-González et al., 2014) or detect knots for wood log sawing (Johansson et al., 2013; Longuetaud et al., 2012; Rais et al., 2017), also allows one to retrieve structural packing details of bulk material (Börzsönyi et al., 2016; Moreno-Atanasio et al., 2010) - provided that the size of the particles is large enough compared to the spatial resolution of the device - and to observe and quantitatively investigate the structural changes for specific flow conditions. X-ray tomography has become relatively popular in the last decade to study structural details, bridges, compaction or arching in three-dimensional

granular packing of mono- or poly-disperse glass beads (Cao et al., 2013; Reimann et al., 2017; Richard et al., 2003; Tsukahara et al., 2008; Weis and Schröter, 2017), packing properties for ellipsoidal or irregular particle systems (Börzsönyi et al., 2016; Kou et al., 2017; Tahmasebi, 2018), porosity topology inside grain bulks (Neethirajan et al., 2008) or shear properties (Handl et al., 2017; Wegner et al., 2014). A recent review listed studies related to the use of X-ray tomography to study granular and porous materials (Moreno-Atanasio et al., 2010). However, it does not refer to gravitational flow studies and it is only recently that few research works investigated silo flow in containers with fixed geometries after natural interruption by clogging or jamming (Börzsönyi et al., 2016; Tsukahara et al., 2008; Wegner et al., 2014) or controlled interruption using an outlet shutter (Grudzien et al., 2012; Stannarius et al., 2019). It is worth mentioning that a large number of scanning interruptions (about 40) was performed in Stannarius et al. (2019) to compare the flow properties of soft hydrogel spheres with hard spherical particles discharged from a bucket with concentric circular outlet. In these experiments, a small discharge height between successive scans, i.e. less than a particle diameter, was needed to qualitatively estimate velocity fields. Note that a recent and interesting approach was based on continuous X-ray radiography acquisition and Fourier-based image processing approach to study particle size and orientation fields during discharge in rectangular silo (Guillard et al., 2017). In this way, the controlled interruption of the flow could be avoided. However, the method is only possible for a silo with the rectangular geometry.

This work extends the X-ray tomography investigations mentioned above thanks to the construction of a versatile experimental system, which can generate different types of flow, ranging from concentric funnel flow to eccentric mass flow. It follows the design principles of the silo presented in Grudzień et al. (2018), but it is adapted for geometrical constraints of the chosen X-ray tomography kit. In order to make further comparison with DEM, the study considered two types of coarse grain materials: sorghum and short-grain white rice, which hold different morphologies but similar mechanical properties, as analysed in Babout et al. (2018). In the majority of the studies cited above, particle segmentation was performed using the watershed method and local volume fraction was evaluated using the Voronoi tessellation (Reimann et al., 2017; Weis and Schröter, 2017). However, the watershed method can lead to under- and over-segmentation. Under-segmentation

occurs when two or more connected objects are not separated, whereas over-segmentation occurs when an object is incorrectly separated into multiple objects. The marker-based watershed (MBW) method used in this study and presented in Babout et al. (2018) reduced significantly the amount of segmentation mistakes.

This work, which uniquely combines the design of a new generation of experimental silo, the possibility offered by X-ray tomography to unambiguously characterize bulk materials and the choice of granular materials to facilitate the comparison between tomography results and DEM simulation, completes previous studies carried out using X-ray imaging or electrical tomography (Babout et al., 2013; Grudzień et al., 2018; Waktola et al., 2018). The main vocation of the paper is to technically demonstrate the applicability of the presented method by presenting results of the evolution of packing in different zones of the silo during concentric/eccentric discharge process of funnel flow of different granular systems. By doing so, it also envisions to make its substantial contribution to the current effort of better understanding granular interaction during silo discharge and therefore, participate to the development of process engineering, mainly linked to container emptying process, which is of importance in the agriculture industry.

2. Materials and Methods

2.1. Granular materials

The paper focuses on two different granular materials, which have been investigated in a previous work (Babout et al., 2018), namely sorghum and short-grain white rice (referred to as rice hereafter). Both physical and mechanical properties have been estimated for the different chosen materials and the most important ones are summarized in Table 1. One can see that the two materials allow to study the influence of the particle shape (sorghum: spheroidal – rice: ellipsoidal) and friction/cohesion properties on discharge dynamics.

Table 1. Granular material properties (Babout et al., 2018).

	Sorghum	Short grain white rice

Tapped density (g/cm^3)	0.83	0.87
Compressibility ratio (%)	8.6	8.6
Average minimum size (mm)	2.5	2
Largest aspect ratio	1.5	3
Young modulus of bulk material (MPa)	3.2	4.5
Natural angle of repose (°)	30.4	33
Internal friction angle (°)	25.4	33.5
Cohesion (kPa)	0.67	0.58
Wall friction angle (°)	13.8	15.7

2.2. Experimental setup

All discharge experiments were carried out using the model silo shown in Figure 1. This versatile silo consists of 5 independent parts, which are indicated in Figure 1a: the base made of brass, the silo bin that can move up and down, the outlet shutter that can move both horizontally and vertically and the two hopper modules mounted on the base that can slide horizontally and have their side plane rotating from 0° to 70°. All parts, which are above the red dashed line in Figure 1a are made of Perspex sheets of 3.5 mm thickness to absorb as few X-rays as possible during tomography scans. The inner part of the bin is 10 cm wide and 7 cm deep. The shutter top has a round ridge shape to assure contact with the bottom edge of the hopper plates in the case of eccentric setting, as it can be seen in Figure 1. With such a design, this versatile silo can adapt to different grain sizes, different discharge speeds and produce different flow patterns (concentric vs. eccentric, mass flow vs. funnel flow). However, this paper concentrates on the study of grain flow dynamics during funnel flow. The configuration of the silo is illustrated in Figure 1b and is mainly concerned with setting parameters *h*, d_1 and *d*, knowing the desired outlet width *w* and hopper angles α_1 and α_2. Detailed mathematical expressions of these silo parameters can be found in the Appendix A. It should be noticed that the fixed dimensions *l* and *e* are identical for both hopper sides and are measured from the centre of the cylindrical hinge indicated in Figure 1b.

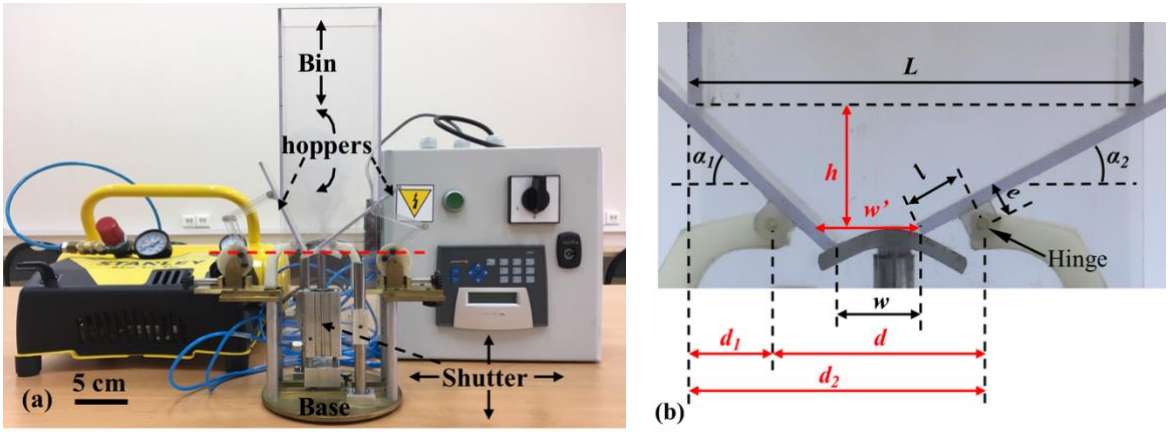

Figure 1. View of the versatile silo model (a) general view with the air compressor and control box. Empty silo in eccentric mass flow configuration (b) enlarged view around the silo outlet with the indication of the parameters to be changed for obtaining a chosen silo geometry (**red** variables are calculated knowing **black** ones).

Regarding the silo monitoring, the opening/closing outlet is remotely controlled using an 8-bar air compressor and in-house control box, as depicted in Figure 1a. The controller can operate opening/closing interval in less than 100 ms with a typical air pressure of 4 bars. With such setting, the discharge process can be controlled outside of the X-ray tomography kit while X-rays are on. Time-lapse X-ray tomography experiments were carried out at the MATEIS laboratory of INSA-Lyon (France) using a Phoenix v|tome|x system equipped with a 160kV/15W X-ray tube. The view of the X-ray cabin is shown in in Figure 2. Experiments related to funnel flow were usually performed with a time interval between 2 successive scans in the [800 – 1500] ms range. Continuous radiographs of the full silo discharge and between successive scans were also compiled for all investigated conditions and animated gif are given as supplementary data. Experimental parameters for the X-ray scan acquisitions are summarized in Table 2. Table 2 also indicates the silo configuration parameters used for the different discharge scenarios, in terms of hopper angles and outlet width. In order to generate eccentric flow, the outlet position is shifted by 8 mm. Moreover, since rice has a larger elongation than sorghum, the outlet was increased to avoid clogging during funnel flow. One can also notice the granular material filling heights (and corresponding weight) were kept similar for all experiments. Reconstructed coronal views of the silo filled with the different granular mixtures for

different flow configurations are shown in Figure 3. All tomographic images were reconstructed using the well-known filtered back projection algorithm.

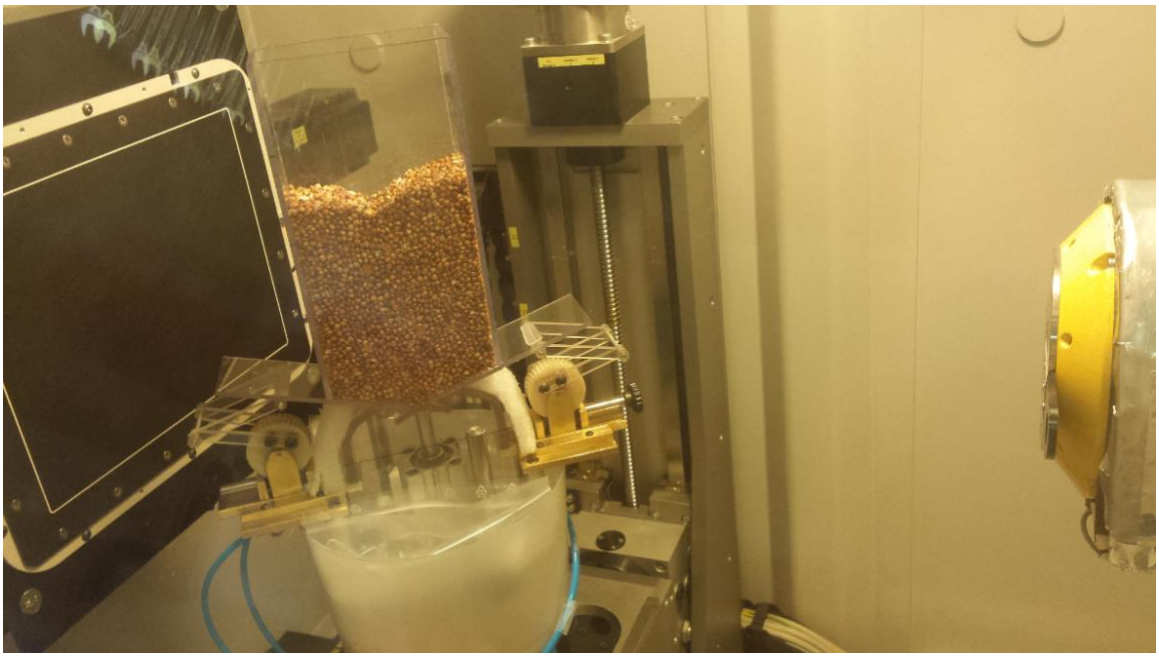

Figure 2. View of the interior of the X-ray tomography kit showing the silo configured for concentric funnel flow (material: sorghum).

Table 2. Experimental parameters for X-ray tomography experiments and silo configuration.

	t (ms)	s_x (μm)	$\alpha_{1/2}$(°)	w (cm)	h_f (cm)	m_g (g)
Sorghum	333	80	20/20	1.4	16.5	693
			20/30			
Rice			20/20	1.7	16.5	689
			20/30			

t: exposure time – s_x: voxel size - $\alpha_{1/2}$: hopper angle (1: left, 2: right) – w: outlet width - h_f: approximate filling height - m_g: granular material weight.

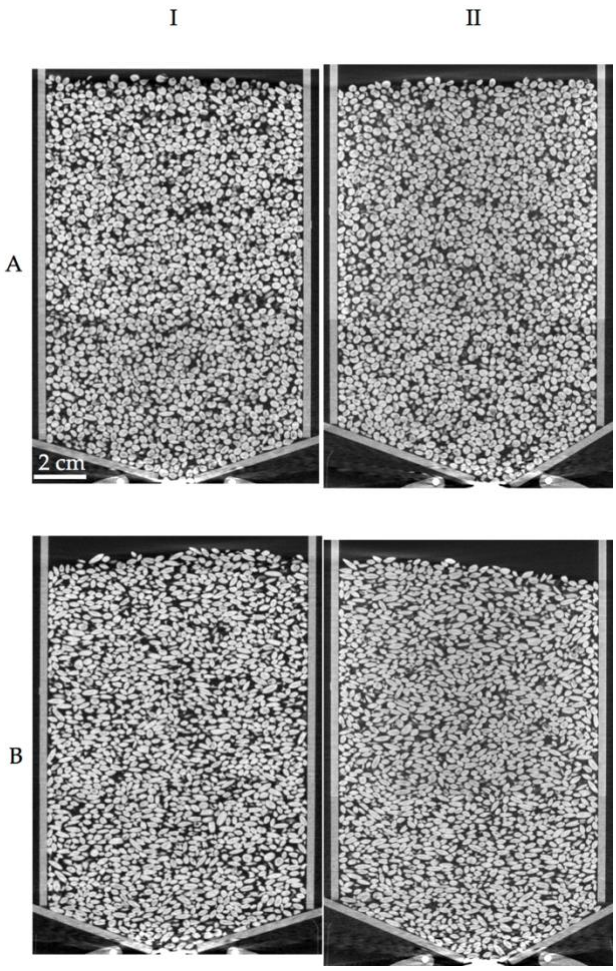

Figure 3. Coronal views of the different granular materials for different silo configuration at silo half-depth after silo filling and prior to first discharge. (A) sorghum, (B), rice. (I) symmetric - low hopper inclination, (II) asymmetric low hopper inclination.

2.3. Image processing strategy

A graphical illustration of the image processing strategy that was employed to extract morphological characteristics of granular packing is shown in Figure 4. Note that the figure presents 2D illustrations for visualisation purposes. However, all digital operations were performed on 3D images. Since the granular materials have been purposely selected to facilitate the study of the flow dynamics at the level of the grains, the evaluation of parameters such as the average or the local packing fraction can only be done if both the silo structure, which is visible in Figure 4a, and the surrounding air are digitally filtered, as shown in Figure 4b-c. All steps, which were developed in Matlab® R2013a and made usage of several functions of the Image Processing Toolbox™, are described in the following sub-sections.

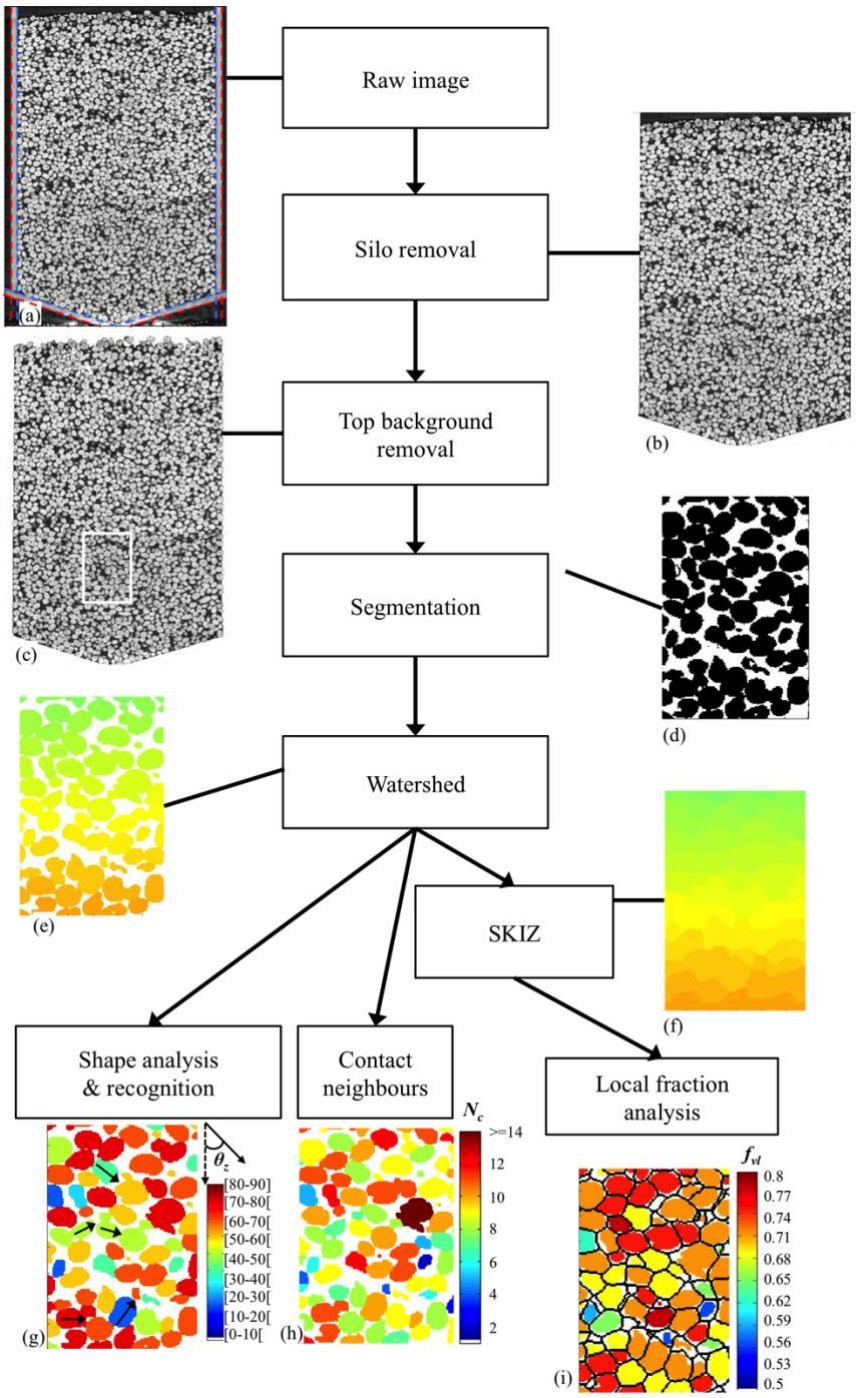

Figure 4. Illustrated flowchart of the image processing steps applied to the X-ray tomography images of granular materials during silo discharge. The white frame in (c) corresponds to the ROIs shown in (d-i).

2.3.1. Silo removal

The first step consists in detecting the edges of the silo structure, since no 3D image of the emptied silo was recorded. Moreover, Perspex and granular materials, especially organic ones, have similar intensity values in the X-ray tomography images. Therefore, it is impossible to apply basic thresholding to only segment the silo structure. Instead, the chosen approach is based on the

reconstruction of surfaces using a three-point edge detection method to retrieve plane equations of the outer and inner sides of the silo wall, both in the bin and hopper parts. The result of such wall detection is indicated by red and blue dashed lines in Figure 4a and the segmentation result following the silo removal is shown in Figure 4b. The silo boundary retrieval is applied 6 times, for the 4 faces of the silo bin and the 2 hopper plates. Finally, the remaining surrounding background, which lies above the upper surface of the granular packing, is removed using a combination of intensity thresholding and erosion/dilation operations. A so-called envelope, that is to say the minimum hull, which contains the granular packing, is finally obtained, as shown in Figure 4c.

2.3.2. Individual grain segmentation

Following these image pre-processing steps, different digital volumetric operations can be performed at the level of the individual grains, ranging from their segmentation to their shape classification, orientation analysis and volume fraction calculation. As far as the segmentation of the grains is concerned, it has been described in details in Babout et al. (2018) and can be summarized as follows: a marker-based watershed (MBW) method, which implements a pre-processing step to select good island markers, is used to separate the grains in contact after the particles have been segmented using thresholding, as illustrated in Figure 4d-e.

2.3.3. Detect grain orientation

In the case of particle orientation change during discharge, the tensor of inertia of each separated and labelled grains is computed, as explained in Waktola et al. (2018) and the corresponding eigenvector of the smallest eigenvalue is chosen as the principal direction. The projection angle θ_z, which corresponds to the angle between the grain axis along its largest dimension and the z-axis, which corresponds to the gravity direction in the 3D images, is used to locally estimate the grain orientation. This is illustrated in Figure 4g, where grains labelled in dark blue or dark red have their main axis lying parallel or perpendicular to the gravity direction, respectively.

2.3.4. Retrieval of coordination number

The labelling following MBW is also useful to estimate the coordination number N_c, i.e. the number of contacting or touching neighbours per particle, as illustrated in Figure 4h. This calculation

is a useful estimation of packing information, but also an indicator of correct volume fraction estimation. The calculation is done in the following way: each label corresponding to a single grain is dilated once and the number of intersections with surrounding labels is the estimation of N_c.

2.3.5. Local volume fraction estimation

The other important image processing path that takes the watershed segmentation result as an input targets the estimation of local volume fraction - another important parameter to analyse flow behaviour during silo discharge. As mentioned in the introduction, numerous studies have used the Voronoi tessellation or Delaunay triangulation to divide the space around particle centroids. However, this approach fails to estimate correctly local volume fraction in the case of poly-dispersed particles in shape and size. Instead, the current work is based on an alternative approach called the skeleton of influence zone (SKIZ) (Herbin et al., 1996; Russ, 1995). The method attributes to every labelled object a nearest neighbourhood of background voxels, known as its zone of influence, as illustrated in Figure 4f. The ratio of the volume of a given labelled particle and its zone of influence is an estimation of the local particle volume fraction f_{vl}. Consequently, one can label particles based on their local volume fraction range, as illustrated in Figure 4i, where blue and red labels mean high and low local voidage, respectively.

3. Results

This section focuses on the comparison of results for the different silo configurations mentioned in the previous section, with a particular focus on material type and concentric/eccentric flow. Particularly, the comparison mainly analyses the local concentration, coordination number and grain orientation evolution during silo discharge and how they change in different parts of the silo i.e. from the wall to the centre of the packing. The results are evaluated at different discharge fraction D_r. Discharge fraction was evaluated in the following manner. It can be calculated from the 3D images by comparing the volume of particles at the given scan s with the initial scan prior to discharge. It should be kept in mind that the discharge fraction is not an evaluation of the discharge rate, since the X-ray tomography measurements were not done in a continuous manner. Note also that this image-based measurement is less accurate than a direct measurement of the discharged material weight using

for instance a load cell. However, such sensor could not be used in the current silo due to space and design restrictions. The average packing density can also be easily estimated from the 3D images. It is simply the average ratio between the volume of particles after watershed separation and the volume of the corresponding zone of influence obtained by the SKIZ method.

3.1. Concentric vs. eccentric flow

Figure 5 shows a comparison between the flow characteristics observed during funnel flow of sorghum for similar outlet width, but different hopper asymmetry to generate concentric and eccentric flows. The figure shows two kinds of images: coronal views in the middle along the silo depth and projection view corresponding to depth packing density integration. The projection view confirms that, from the average point of view, the chosen coronal views are representative of grains behaviour throughout the depth of the silo. While Figure 5a shows well-known characteristics of concentric flow with a contractancy/dilatancy effect at the beginning of the discharge (D_r=0.065) and the presence of symmetric dense stagnant zones that decrease in size during discharge, the flow dynamic reveals interesting insights in the case of the eccentric flow. Firstly, the fact that the outlet is moved to the right by 8 mm w.r.t the bin position because of the hopper angle asymmetry creates a left stagnant zone, which is larger than in the case of the concentric flow. More interestingly, the right stagnant zone is replaced by a dense flow zone, which moves downward along the right silo wall. This dense flow zone disappears when the discharge fraction reaches about 0.5. An indicator of the dense flow zone is the presence of loosely packed granular material at its bottom at the level of the hopper. In both scenarios, there is a difference of about 6-8% between the looser and denser zones, the denser zones having a packing density of about 0.68 in average.

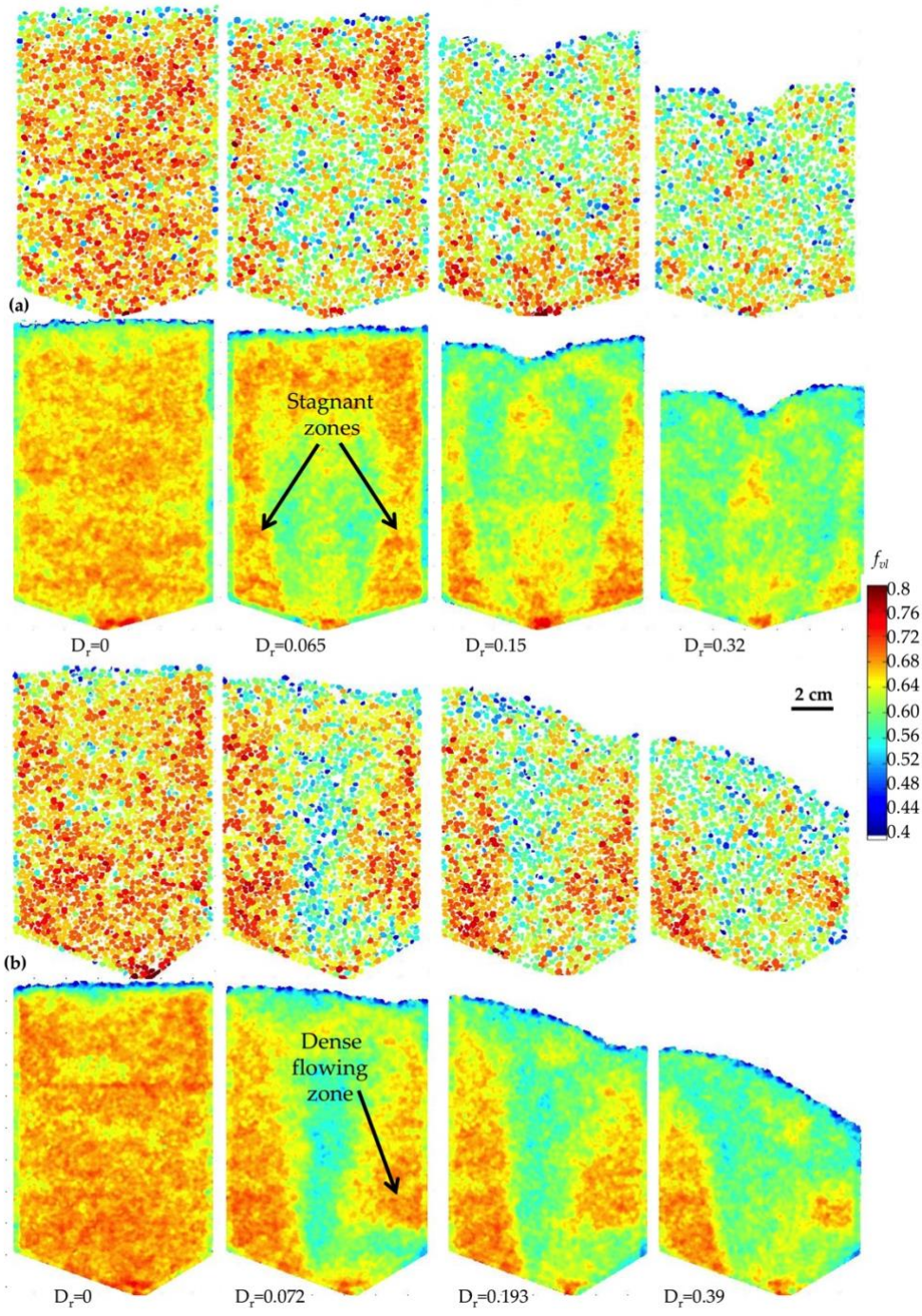

Figure 5. Coronal views chosen in the middle along the silo depth (first row) and depth projection (second row) showing local volume fraction evolution at different discharge fractions for sorghum material in the case of funnel flow. (a) symmetric hoppers (20°-20°), (b) asymmetric hoppers (20°-30°). Outlet width: *w*=14 mm.

3.2. Effect of grain aspect ratio

Figure 6 shows a similar representation of the discharge sequences than Figure 5, but for rice. Note that the outlet width was wider by 3 mm to avoid possible clogging, which was observed for rice when it is set as in the case of sorghum. One can notice in Figure 6a that, surprisingly, rice showed

an eccentric discharge in the case of the symmetric hopper setting for D_r<0.2, then the discharge tends to settle into a concentric flow. Three different continuous discharge experiments were carried out with the same setup and the flow characteristics were very similar. As far as the asymmetric setup is concerned in Figure 6b, the flow exhibits similar behaviour than in the previous rice case and the sorghum case with asymmetric hopper setup, with the presence of the denser flow zone in the right part of the silo above the hopper inclined at 30°. The eccentric V-shape free surface also forms but at a higher discharge fraction (i.e. between 0.5 and 0.6). However, it is also interesting to see how the distribution of rice grains orientation evolves in the packing during discharge.

Figure 7 shows the comparison between packing density (f_{vl}), coordination number (N_c) and grain orientation (θ_z) maps in the middle coronal view in the case of rice for the asymmetric setting, at a discharge fraction that clearly presents different clusters of grain concentration and particle orientation in the flowing zone. The changes in the distribution of grain orientation is more visible in the case of rice, as it can be deduced by comparing the grain orientation distribution of sorghum and rice shown in Figure 8. This scan corresponds to an interruption between the 2nd and the 3rd images of Figure 6b (D_r=0.228) and the presented views shown in Figure 7 are representative for the whole depth of the silo. Moreover, Figure 7a shows a continuity in the distribution of f_{vl}, when compared with the 2nd image of Figure 6b. The combination of packing density and grain orientation maps reveals 5 main regions of interest indexed in Figure 7a: the stagnant zone (#1) and 4 regions in the flow zones (#2-5). The denser packing of the stagnant zone, which also corresponds to larger N_c, and the lower packing density of the funnel zones #2-3 relate relatively well with the natural nearly horizontal material settlement and the gravity-driven horizontal-to-vertical re-orientation of the grains towards the outlet, respectively. However, the remaining two regions need more consideration to explain their characteristics. Region #4 presents very similar characteristics than region #1 in terms of f_{vl}, N_c and θ_z ranges. Moreover, its suggested location and width also fit well with the position of the right hopper inclined at 30°, as it was already mentioned above in the case of sorghum. The hopper angle increase may have an impact on the packing stability, which changes it from a stagnant zone into a dense flowing zone or mass flow zone. Consequently, grains in region #5 present in average a similar orientation than those of region #4 with a lower packing density. This is possibly generated

by the proximity of the hopper part and its low inclination compared to the mass flow case, which reduce the rotational momentum of the grains.

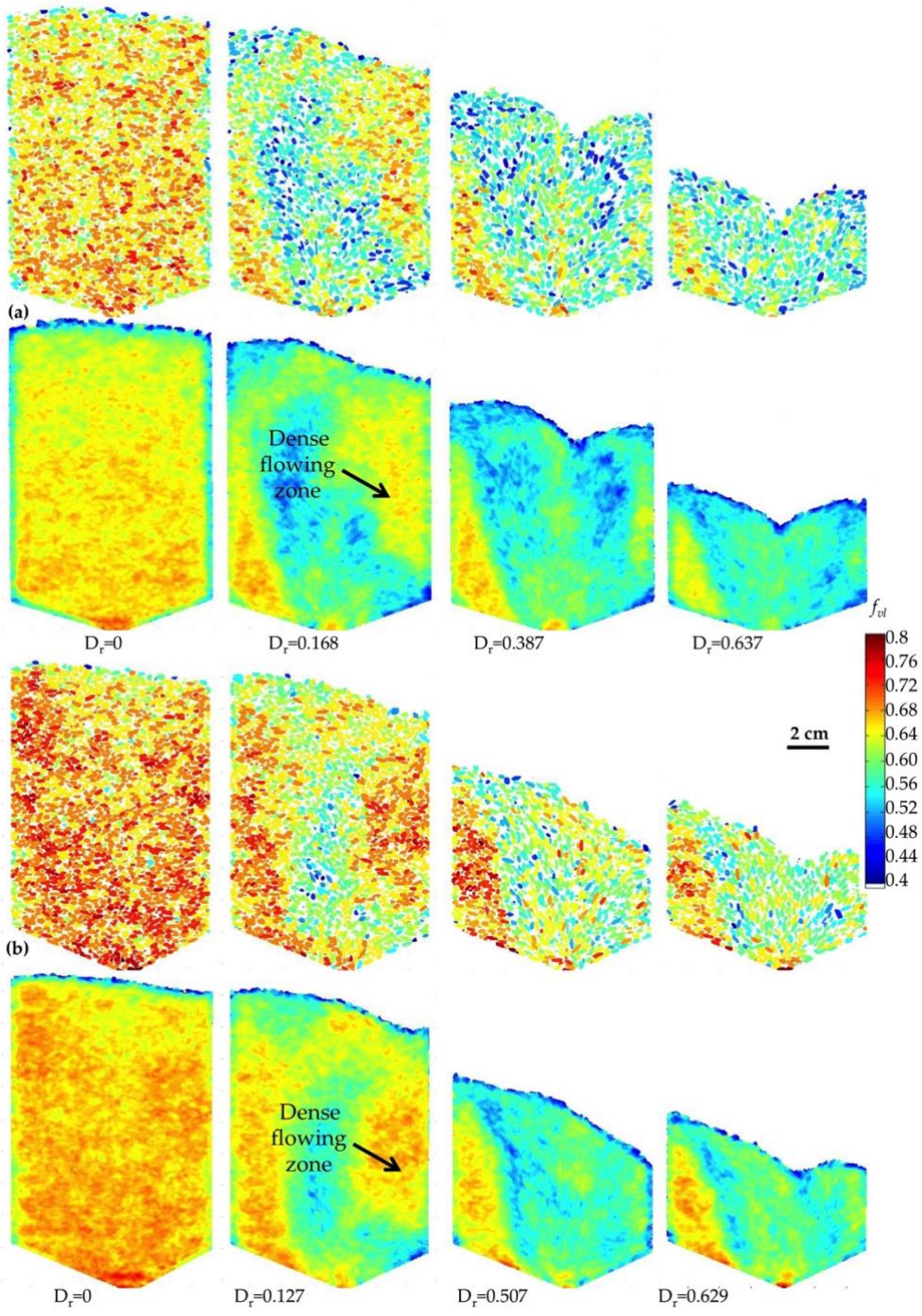

Figure 6. Coronal views chosen in the middle along the silo depth (first row) and depth projection (second row) showing local volume fraction evolution at different discharge fractions for rice material in the case of funnel flow. (a) symmetric hoppers (20°-20°), (b) asymmetric hoppers (20°-30°). Outlet width: *w*=17 mm.

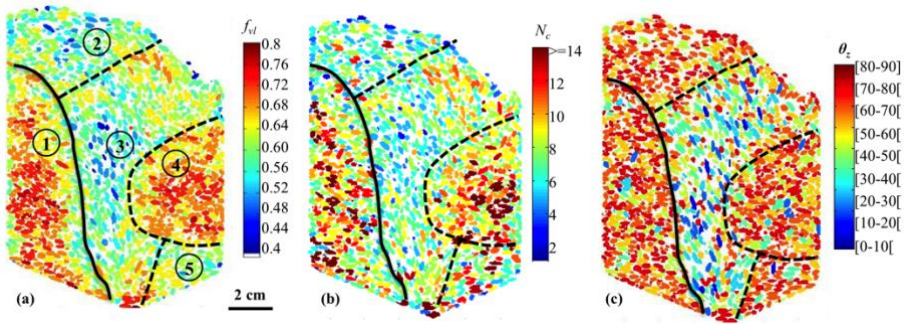

Figure 7. Comparison between local packing density, contact neighbours and particle orientation angle in the case of eccentric funnel flow of rice material for D_r=0.228 (Outlet width: w=14 mm). (a) coronal view of density packing in middle plane, (b) corresponding contact neighbours map, (c) corresponding orientation map. Angle between principal direction and z-axis (vertical direction on the figure). In all pictures are delineated the boundary separating the stagnant and the flowing zones (solid line) and special regions in the flowing zone (dashed lines).

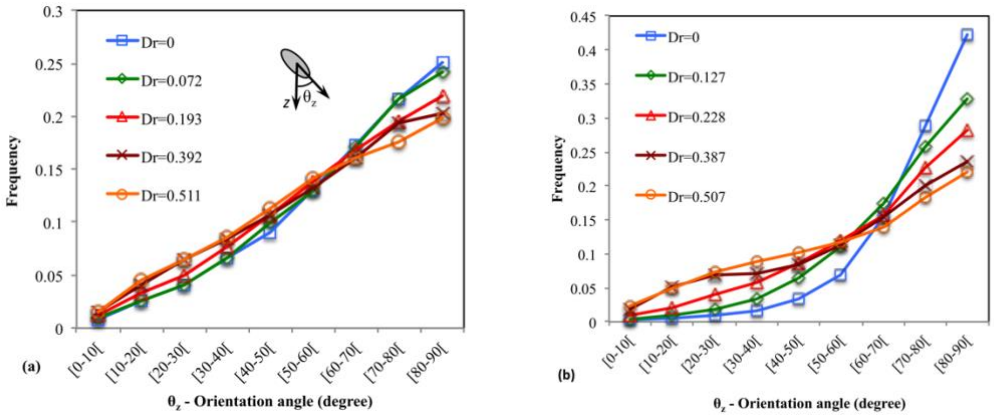

Figure 8. Distribution of orientation angle for the asymmetric setup for different discharge fractions. (a) sorghum, (b) rice.

The evolution of frequency distribution of the coordination number N_c as a function of the discharge fraction also indicates changes occurring in the packing during funnel flow of sorghum and rice. As shown in Figure 9, the distributions, which originally are mostly unimodal – sorghum in symmetric setup shows a bimodal distribution with peaks maximum at N_c=6 and N_c=8 - have their peak position shifted towards lower N_c while discharge takes place. Unimodal to bi- or even tri-modal decomposition of the distributions also often occur in the different scenarios. In the case of sorghum (Figure 9a-b), one can notice that the shift operates from N_c=8 to N_c=6, which can be interpreted, by analogy to cubic crystal system, to a change from body-centred cubic to primitive cubic packing

during discharge mainly occurring in the flow zone. In the case of the symmetric setup (Figure 9a), one can notice the transition from a bi-modal to a unimodal distribution, which indicates that the funnel flow "loosens" the packing structure. Therefore, for D_r>0, the right peak can be associated with the stagnant zone, which present larger packing density. This is also in agreement with the packing density maps shown in Figure 5a. Similar observations are also valid for rice, with the difference that the mean of the peaks are larger by roughly 1, which is linked with a larger aspect ratio of the rice grains. The increase is logical since with the additional orientational degrees of freedom introduced by particle elongation, more contact points are required than in the case of packing of granular material with lower aspect ratio (Alexander, 1998).

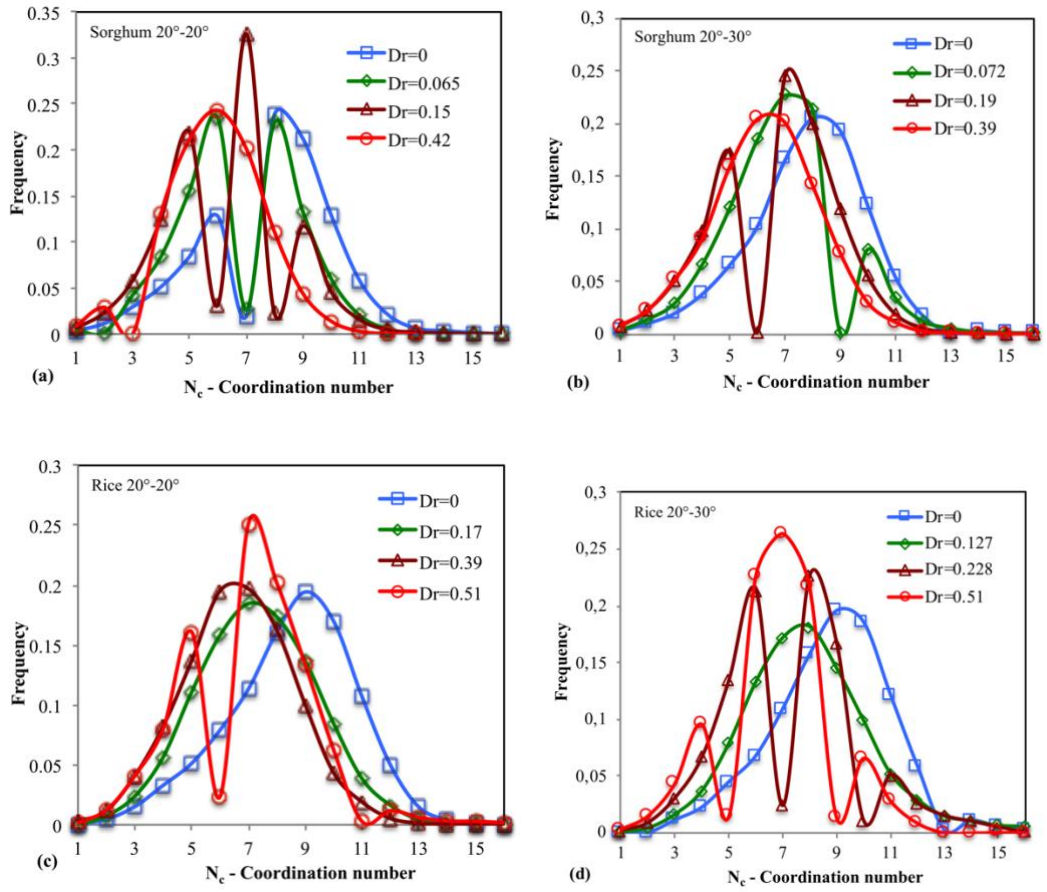

Figure 9. Distribution of the coordination number for all funnel flow experiments for different discharge fractions. (a) sorghum – symmetric setup, (b) sorghum – asymmetric setup, (c) rice – symmetric setup and (d) rice - asymmetric setup.

4. Discussion

The content of this paper presents, according to the authors' knowledge, different levels of novelty, which concern the experimental protocol and the generated qualitative and quantitative results. Before going into the interpretation of the results, one should question the different steps of the process, from data acquisition towards its interpretation.

4.1. Can the experimental protocol be trusted?

The type of rectangular versatile silo presented in this paper allows to investigate different types of flow regimes with a single apparatus. Its design, which consists of the positioning of different elements of the structure, i.e. the bin, the hoppers and the outlet induces a loss of structural integrity due to the "loose contact" between the hopper plates and the bin. Indeed, prior to filling, it was checked that the contact is made between the elements. However, after filling, the weight of the granular material may induce sagging of the hopper plates, creating a disconnection with the bin. This can be noticed in Figure 3 (case II-B, right bin border). When it occurred, no particle escape was observed because the created slots never exceeded more that 2 mm in height and no change in the flow pattern and the flow was observed from the radiography sequences acquired during continuous discharges or between successive X-ray tomography scans. Therefore, it was concluded that this problem does not impact on the observed results.

As it was mentioned in section 2.2, time-lapse X-ray tomography experiments consist in multiple flow interruptions during one discharge experiment to acquire tomography scans. The time window between successive outlet opening and closing was between 800 and 1500 ms and judged sufficient to observe flow changes during discharge. However, it was observed that the outlet closing induced in some extent packing settlement and material compaction occurred, with the maximum height of the material packing contracted by around 1 grain size (around 2-4 mm). Therefore, the density quantification, from the measurement perspective, overestimates the real density changes during the flow. Nonetheless, the characteristics of the concentration changes, as well as the overall rotation of the grains are not impacted by the process interruption. Moreover, the continuous and interrupted sequences of radiography recorded for the 4 experimental conditions also present repeatable flow characteristics (see the supplementary data), which validate the approach of the flow interruption. Similar situation occurred in some extent with the X-ray tomography experiments presented in

Börzsönyi et al. (2016), which investigated elongated particle rotation during funnel flow in flat bottom silo stopped by clogging.

4.2. Can the image processing approach be trusted?

As it was mentioned in sections 1 and 2.3, the marker-based watershed (MBW) method used in this work reduced significantly the amount of segmentation mistakes, but could not eradicate them, leaving around 10% of grains not satisfyingly segmented (Babout et al., 2018). Alternatively, another segmentation step based on feature recognition was incorporated in the algorithm to reduce the number of under-segmented grains. In a nutshell, the method relies on calculating shape descriptors presented in Babout et al. (2018), namely aspect ratios F_{ab} and F_{ac} and an ellipsoid goodness of fit parameter γ. Then, it uses a density-based cluster analysis approach to select segmented objects, which do not belong to the largest class. These are retreated individually using MBW to eventually separate objects, which were omitted in the first call of the watershed. Segmentation verification showed a steep decrease of the unsatisfyingly segmented grains by around 60%. However, the comparison between the 2 methods did not show particular difference in the case of packing density and orientation analysis, since the quantitative analysis concerned average evolutions. However, in the case of individual grain analysis, the 2-step MBW method should be used.

Another aspect of the image processing analysis is the trustfulness in the local volume fraction estimation based on the SKIZ method. This highly relates to the value of the segmentation threshold. Investigation showed that a variation of ±10 around the chosen common intensity value used to segment all sorghum and rice volumetric images induces a change of ±1.5% in the average volume fraction calculation. This is in line with the initial packing density presented in different figures of this article (i.e. Figure 5-7), where values oscillate between 0.63 and 0.66. This range value is in agreement with what can be expected, oscillating around irregular packing (0.64) (Chaikin, 2007). Another confirmation about the measurement reliability is the values of the coordination number obtained prior to discharge. Simulated results presented in Gan et al. (2016) shows that for coarse particles (1 mm diameter) with aspect ratio ranging between 1.5 and 3, N_c varies between 6.8 and 7.3 and values increase with size. The N_c values summarized in Table 3 follows these trends, since the

mean value for rice is ~8.7, while it is around 7.7 for sorghum, and both grain materials have an average size larger than the maximum simulated size mentioned above (see Table 1).

As far as the grains' orientation is concerned, calculated values are also in line with expectations. For instance, the scatter of orientation after silo filling shown in Table 3, regardless of the hopper angles, is smaller for rice than sorghum with standard deviation of ~13.5% and ~19.5%, respectively. This proves that the estimated measurements could be trusted.

Table 3. Comparison of initial grains orientation and coordination number (mean μ, standard deviation σ) for the different experiments before first discharge.

		Hopper angles (°)	20-20	20-30
Sorghum	θ_z	μ (°)	65.6	64.7
		σ (°)	19.4	19.4
	N_c	μ	7.7	7.8
		σ	2.2	2.1
Rice	θ_z	μ (°)	74.2	74
		σ (°)	13.5	13.7
	N_c	μ	8.5	8.9
		σ	2.2	2.3

4.3. Significance of the research

The main vocation of the article is to present a new experimental protocol and demonstrate its applicability to study granular flow in silos. Even if one time-lapse X-ray tomography experiment was carried out for each of the 4 experimental conditions presented in this work and may be judged insufficient to draw general conclusions, the good agreement between the continuous and interrupted sequences of radiography presented as supplementary material supports the trustfulness of the results.

In that context, the discharge experiments carried out for sorghum and rice reveal interesting results. One is the appearance of dense flow zone in the case of eccentric discharge and the influence of particle elongation to extend the effect for symmetric hopper setting. Jenike maps for flow mode prediction indicate that for the range of wall friction and internal friction angles of sorghum and rice

(see Table 1), the transition from mass to funnel flow would occur for hopper angle lower than 45° (Jenike, 1961; Ketterhagen et al., 2009). Therefore, the hopper angles are in agreement with funnel flow mode, even in the eccentric case. However, hopper asymmetry, for a fixed bin width, creates changes in the stagnant zone widths: while the stagnant zone above the smaller hopper angle increases, the one above the larger hopper is shrank, even removed if it cannot withstand wall slip. This is possibly what happens in the current experiment with sorghum and rice, as the outlet displacement of 8 mm is roughly half of the stagnant zone width at mid-height in the case of concentric funnel flow (e.g. see Figure 5a). Moreover, the fact that the width of silo (10 cm) is roughly 30 times larger than the average grain size, may also accentuate the effect. Combined factors may be the major causes of the stagnant zone to change into a flowing zone of similar packing density and orientation. More work needs to be carried out to confirm this observation, especially in the case of symmetric setting where this eccentric discharge was also observed for rice.

The presented work opens new avenues in terms of silo discharge investigation, especially for comparison with simulation. Work is under way to model the experiments presented in this paper using discrete element modelling (Miśkiewicz et al., 2018). Since exact positioning of the sorghum or rice grains, which can be modelled by prolates, can be directly used in the proposed approach, structurally faithful simulation can be generated and directly compared with X-ray tomography data, to investigate predicted packing density and grain orientation changes at different scales (i.e. globally, locally or at the level of individual grains).

5. Conclusions

The following conclusions can be drawn from the present study, which was mainly foreseen to demonstrate the applicability of time-lapse tomography and subsequent image processing and analysis steps to study granular flow of coarse grains in silos:

- Two organic cohesionless materials, sorghum and rice, with relatively similar physico-mechanical properties but different morphologies were investigated during silo discharge. Their large size, which is roughly 30 times larger than the spatial resolution

of the chosen X-ray tomography device facilitated their study during the discharge processes.

- In order to investigate different flow modes, ranging from funnel flow to mass flow, a single versatile silo structure was developed, which gives the possibility to regulate independently the hopper angles and outlet width to adapt to different granular materials size and flow considerations. The silo dimensions were also thought to fit the structure into conventional X-ray tomography cabin and perform its monitoring remotely. Despite dimensions that do not reflect real silo sizes found in the agriculture, this experimental stand is considered as a good compromise to allow the comparison between three dimensional experimental results and numerical predictions.
- The application of a marker-based watershed approach to individually segment the grains in the 3D images was found particularly useful to extract meaningful local geometrical parameters, such as coordination number, packing density and orientations. These are the three principal parameters used in this work to study flow dynamics during silo discharge.
- The work focused on concentric and eccentric discharge processes of funnel flow. Even if two hopper angle conditions, i.e. 20°-20° and 20°-30°, were investigated and one time-lapse experiment performed per case seems limited to draw general conclusions, interesting results were revealed, mainly for the eccentric cases. Indeed, hopper angle asymmetry seems to create the main effect on flow dynamics, with the creation of a dense flowing zone instead of stagnant zone along the silo side with the largest hopper inclination, which has similarities with mass flow. The observed effects were amplified for elongated grains. The proportionality of few dozen between the average grain size and the silo width may have an impact on the stagnant zone disappearance in the eccentric case. Similar observation for rice in the case of symmetric hopper setting is still a matter of discussion.
- The coordination number is a good indicator of the reliability of the proposed image processing approach to study flow dynamics during silo discharge. The stagnant and the

flowing zones of the funnel flow mode exhibit different coordination number distributions, which have a direct effect on different packing densities between the 2 zones.

Work is in progress to investigate the individual behaviour of tracer particles inserted in granular packing. The comparison of flow characteristics with DEM, for instance particle trajectories during silo discharge or the packing density evolution presented in this research, are under way. These will give a broader understanding about physical phenomena observed in the bulk of granular materials subjected to silo discharge.

Acknowledgments:

This research was funded by the National Science Centre in Poland (grant number: 2015/19/B/ST8/02773).

6. Appendix A

Silo configuration parameters indicated in Figure 1b and mentioned in section 2.2 can be easily calculated using the following expressions:

$$d = w + l\left(\cos\left(\alpha_1\right) + \cos\left(\alpha_2\right)\right) + e\left(\sin\left(\alpha_1\right) + \sin\left(\alpha_2\right)\right) \tag{A1}$$

$$h = \frac{L - d + e\left(1/\sin\left(\alpha_1\right) + 1/\sin\left(\alpha_2\right)\right)}{1/\tan\left(\alpha_1\right) + 1/\tan\left(\alpha_2\right)} \tag{A2}$$

$$d_1 = \frac{h - e/\cos\left(\alpha_1\right)}{\tan\left(\alpha_2\right)} \tag{A3}$$

$$w' = w + l\left|\cos\left(\alpha_1\right) - \cos\left(\alpha_2\right)\right|\tan\left(\alpha_2\right) \quad \text{for} \quad \alpha_2 \geq \alpha_1 \tag{A4}$$

where L is the silo width, w is the outlet width, e is the normal distance between the inner or top side of the hopper plate and the principal axis of the cylindrical hinge, l is the length of the hopper

extension from the centre of the cylindrical hinge, α_1 and α_2 are the angles of the left and right hoppers, respectively.

7. References

Alexander, S., 1998. Amorphous solids: their structure, lattice dynamics and elasticity. Phys. Rep. 296, 65–236. https://doi.org/10.1016/S0370-1573(97)00069-0

Ayuga, F., Guaita, M., Aguado, P., 2001. Discharge and the eccentricity of the hopper influence on the silo wall pressures. J. Eng. Mech. 127, 1067–1074.

Babout, L., Grudzien, K., Maire, E., Withers, P.J., 2013. Influence of wall roughness and packing density on stagnant zone formation during funnel flow discharge from a silo: An X-ray imaging study. Chem. Eng. Sci. 97, 210–224. https://doi.org/10.1016/j.ces.2013.04.026

Babout, L., Grudzień, K., Wiącek, J., Niedostatkiewicz, M., Karpiński, B., Szkodo, M., 2018. Selection of material for X-ray tomography analysis and DEM simulations: comparison between granular materials of biological and non-biological origins. Granul. Matter 20, 38. https://doi.org/10.1007/s10035-018-0809-y

Balevičius, R., Sielamowicz, I., Mróz, Z., Kačianauskas, R., 2011. Investigation of wall stress and outflow rate in a flat-bottomed bin: A comparison of the DEM model results with the experimental measurements. Powder Technol. 214, 322–336. https://doi.org/10.1016/j.powtec.2011.08.042

Börzsönyi, T., Somfai, E., Szabó, B., Wegner, S., Mier, P., Rose, G., Stannarius, R., 2016. Packing,

alignment and flow of shape-anisotropic grains in a 3D silo experiment. New J. Phys. 18, 093017. https://doi.org/10.1088/1367-2630/18/9/093017

Brecht, J.K., Shewleft, R.L., Garner, J.C., Tollner, E.W., 1991. Using x-ray-computed tomography to nondestructively determine maturity of green tomatoes. Hortscience 26, 45–47.

Cao, Y.X., Chakrabortty, B., Barker, G.C., Mehta, A., Wang, Y.J., 2013. Bridges in three-dimensional granular packings: Experiments and simulations. EPL (Europhysics Lett. 102, 24004. https://doi.org/10.1209/0295-5075/102/24004

Chaikin, P., 2007. Random thoughts. Phys. Today 60, 8–9. https://doi.org/10.1063/1.2754580

Cheng, Y.M., Chau, K.T., Xiao, L.J., Li, N., 2010. Flow Pattern for a Silo with Two Layers of Materials with Single or Double Openings. J. Geotech. Geoenvironmental Eng. 136, 1278–1286. https://doi.org/10.1061/(ASCE)GT.1943-5606.0000334

Chou, C.S., Hsu, J.Y., Lau, Y.D., 2002. The granular flow in a two-dimensional flat-bottomed hopper with eccentric discharge. Phys. A Stat. Mech. its Appl. 308, 46–58. https://doi.org/10.1016/S0378-4371(01)00628-8

Donis-González, I.R., Guyer, D.E., Pease, A., Barthel, F., 2014. Internal characterisation of fresh agricultural products using traditional and ultrafast electron beam X-ray computed tomography imaging. Biosyst. Eng. https://doi.org/10.1016/j.biosystemseng.2013.07.002

Fullard, L.A., Breard, E.C.P., Davies, C.E., Godfrey, A.J.R., Fukuoka, M., Wade, A., Dufek, J., Lube, G., 2019. The dynamics of granular flow from a silo with two symmetric openings. Proc. R.

Soc. A Math. Phys. Eng. Sci. 475, 20180462. https://doi.org/10.1098/rspa.2018.0462

Gan, J.Q., Yu, A.B., Zhou, Z.Y., 2016. DEM simulation on the packing of fine ellipsoids. Chem. Eng. Sci. 156, 64–76. https://doi.org/10.1016/j.ces.2016.09.017

González-Montellano, C., Ramírez, Á., Gallego, E., Ayuga, F., 2011. Validation and experimental calibration of 3D discrete element models for the simulation of the discharge flow in silos. Chem. Eng. Sci. 66, 5116–5126. https://doi.org/10.1016/j.ces.2011.07.009

Grudzień, K., Chaniecki, Z., Babout, L., 2018. Study of granular flow in silo based on electrical capacitance tomography and optical imaging. Flow Meas. Instrum. 62, 186–195. https://doi.org/10.1016/j.flowmeasinst.2017.11.001

Grudzien, K., Niedostatkiewicz, M., Adrien, J., Maire, E., Babout, L., 2012. Analysis of the bulk solid flow during gravitational silo emptying using X-ray and ECT tomography. Powder Technol. 224, 196–208. https://doi.org/10.1016/j.powtec.2012.02.054

Guillard, F., Marks, B., Einav, I., 2017. Dynamic X-ray radiography reveals particle size and shape orientation fields during granular flow. Sci. Rep. 7, 8155. https://doi.org/10.1038/s41598-017-08573-y

Handl, L., Torbahn, L., Spettl, A., Schmidt, V., Kwade, A., 2017. Structural analysis and tracking of micron-sized glass particles during shear deformation: A study based on time-resolved tomographic data. Adv. Powder Technol. 28, 1920–1929. https://doi.org/10.1016/j.apt.2017.05.002

Herbin, M., Bonnet, N., Vautrot, P., 1996. A clustering method based on the estimation of the probability density function and on the skeleton by influence zones. Application to image processing. Pattern Recognit. Lett. 17, 1141–1150. https://doi.org/10.1016/0167-8655(96)00085-2

Jenike, A.W., 1961. Bulletin 108: Gravity flow of bulk solids. University of Utah, Salt lake City.

Johansson, E., Johansson, D., Skog, J., Fredriksson, M., 2013. Automated knot detection for high speed computed tomography on Pinus sylvestris L. and Picea abies (L.) Karst. using ellipse fitting in concentric surfaces. Comput. Electron. Agric. 96, 238–245. https://doi.org/10.1016/j.compag.2013.06.003

Ketterhagen, W.R., Curtis, J.S., Wassgren, C.R., Hancock, B.C., 2009. Predicting the flow mode from hoppers using the discrete element method. Powder Technol. 195, 1–10. https://doi.org/10.1016/j.powtec.2009.05.002

Kou, B., Cao, Y., Li, J., Xia, C., Li, Z., Dong, H., Zhang, A., Zhang, J., Kob, W., Wang, Y., 2017. Granular materials flow like complex fluids. Nature. https://doi.org/10.1038/nature24062

Longuetaud, F., Mothe, F., Kerautret, B., Krähenbühl, A., Hory, L., Leban, J.M., Debled-Rennesson, I., 2012. Automatic knot detection and measurements from X-ray CT images of wood: A review and validation of an improved algorithm on softwood samples. Comput. Electron. Agric. 85, 77–89. https://doi.org/10.1016/j.compag.2012.03.013

Maiti, R., Das, G., Das, P.K., 2016. Experiments on eccentric granular discharge from a quasi-two-dimensional silo. Powder Technol. 301, 1054–1066.

https://doi.org/10.1016/j.powtec.2016.07.054

Medina, A., Cabrera, D., López-Villa, A., Pliego, M., 2014. Discharge rates of dry granular material from bins with lateral exit holes. Powder Technol. 253, 270–275. https://doi.org/10.1016/j.powtec.2013.11.027

Miśkiewicz, K., Banasiak, R., Niedostatkiewicz, M., Grudzień, K., Babout, L., 2018. An algorithm to generate high dense packing of particles with various shapes. MATEC Web Conf. 219, 05004. https://doi.org/10.1051/matecconf/201821905004

Moreno-Atanasio, R., Williams, R.A., Jia, X., 2010. Combining X-ray microtomography with computer simulation for analysis of granular and porous materials. Particuology 8, 81–99. https://doi.org/x10.1016/j.partic.2010.01.001

Neethirajan, S., Jayas, D.S., White, N.D.G., Zhang, H., 2008. Investigation of 3D geometry of bulk wheat and pea pores using X-ray computed tomography images. Comput. Electron. Agric. 63, 104–111. https://doi.org/10.1016/j.compag.2008.01.019

Oldal, I., Keppler, I., Csizmadia, B., Fenyvesi, L., 2012. Outflow properties of silos: The effect of arching. Adv. Powder Technol. 23, 290–297. https://doi.org/10.1016/j.apt.2011.03.013

Rais, A., Ursella, E., Vicario, E., Giudiceandrea, F., 2017. The use of the first industrial X-ray CT scanner increases the lumber recovery value: case study on visually strength-graded Douglas-fir timber. Ann. For. Sci. 74, 28. https://doi.org/10.1007/s13595-017-0630-5

Reimann, J., Vicente, J., Brun, E., Ferrero, C., Gan, Y., Rack, A., 2017. X-ray tomography

investigations of mono-sized sphere packing structures in cylindrical containers. Powder Technol. 318, 471–483. https://doi.org/10.1016/j.powtec.2017.05.033

Richard, P., Philippe, P., Barbe, F., Bourlès, S., Thibault, X., Bideau, D., 2003. Analysis by x-ray microtomography of a granular packing undergoing compaction. Phys. Rev. E 68, 020301. https://doi.org/10.1103/PhysRevE.68.020301

Russ, G.C., 1995. The imaging processing handbook, 2nd ed. CRC Press, Boca Raton.

Rycroft, C.H., Grest, G.S., Landry, J.W., 2006. Analysis of granular flow in a pebble-bed nuclear reactor. Phys. Rev. E 74, 021306.

Sadowski, A.J., Rotter, J.M., 2011. Buckling of very slender metal silos under eccentric discharge. Eng. Struct. 33, 1187–1194. https://doi.org/10.1016/j.engstruct.2010.12.040

Saleh, K., Golshan, S., Zarghami, R., 2018. A review on gravity flow of free-flowing granular solids in silos – Basics and practical aspects. Chem. Eng. Sci. 192, 1011–1035. https://doi.org/10.1016/j.ces.2018.08.028

Sielamowicz, I., Blonski, S., Kowalewski, T.A., 2005. Optical technique DPIV in measurements of granular material flows, Part 1 of 3—plane hoppers. Chem. Eng. Sci. 60, 589–598. https://doi.org/10.1016/j.ces.2004.07.135

Sielamowicz, I., Czech, M., Kowalewski, T.A., 2011. Empirical analysis of eccentric flow registered by the DPIV technique inside a silo model. Powder Technol. 212, 38–56. https://doi.org/10.1016/j.powtec.2011.04.022

Sielamowicz, I., Czech, M., Kowalewski, T.A., 2010. Empirical description of flow parameters in eccentric flow inside a silo model. Powder Technol. 198, 381–394. https://doi.org/10.1016/j.powtec.2009.12.003

Slominski, C., Niedostatkiewicz, M., Tejchman, J., 2007. Application of particle image velocimetry (PIV) for deformation measurement during granular silo flow. Powder Technol. 173, 1–18. https://doi.org/10.1016/j.powtec.2006.11.018

Stannarius, R., Sancho Martinez, D., Finger, T., Somfai, E., Börzsönyi, T., 2019. Packing and flow profiles of soft grains in 3D silos reconstructed with X-ray computed tomography. Granul. Matter 21. https://doi.org/10.1007/s10035-019-0910-x

Steingart, D.A., Evans, J.W., 2005. Measurements of granular flows in two-dimensional hoppers by particle image velocimetry. Part I: Experimental method and results. Chem. Eng. Sci. 60, 1043–1051. https://doi.org/10.1016/j.ces.2004.09.066

Szabó, B., Kovács, Z., Wegner, S., Ashour, A., Fischer, D., Stannarius, R., Börzsönyi, T., 2018. Flow of anisometric particles in a quasi-two-dimensional hopper. Phys. Rev. E 97, 062904. https://doi.org/10.1103/PhysRevE.97.062904

Tahmasebi, P., 2018. Packing of discrete and irregular particles. Comput. Geotech. 100, 52–61. https://doi.org/10.1016/j.compgeo.2018.03.011

Tsukahara, M., Mitrovic, S., Gajdosik, V., Margaritondo, G., Pournin, L., Ramaioli, M., Sage, D., Hwu, Y., Unser, M., Liebling, T.M., 2008. Coupled tomography and distinct-element-method approach to exploring the granular media microstructure in a jamming hourglass. Phys. Rev. E

77, 061306. https://doi.org/10.1103/PhysRevE.77.061306

Waktola, S., Bieberle, A., Barthel, F., Bieberle, M., Hampel, U., Grudzień, K., Babout, L., 2018. A new data-processing approach to study particle motion using ultrafast X-ray tomography scanner: case study of gravitational mass flow. Exp. Fluids 59, 69. https://doi.org/10.1007/s00348-018-2523-2

Wegner, S., Stannarius, R., Boese, A., Rose, G., Szabó, B., Somfai, E., Börzsönyi, T., 2014. Effects of grain shape on packing and dilatancy of sheared granular materials. Soft Matter 10, 5157. https://doi.org/10.1039/c4sm00838c

Weis, S., Schröter, M., 2017. Analyzing X-ray tomographies of granular packings. Rev. Sci. Instrum. 88, 051809. https://doi.org/10.1063/1.4983051

Zhou, Y., Lagrée, P.-Y., Popinet, S., Ruyer, P., Aussillous, P., 2017. Experiments on, and discrete and continuum simulations of, the discharge of granular media from silos with a lateral orifice. J. Fluid Mech. 829, 459–485. https://doi.org/10.1017/jfm.2017.543